JACS
JOURNAL OF THE AMERICAN CHEMICAL SOCIETY

ARTICLE

pubs.acs.org/JACS

Aluminum Foils: The Contrasting Characters of Hyperconjugation and Steric Repulsion in Aluminum Dimetallocenes

Katherine R. Compaan, Jeremiah J. Wilke, and Henry F. Schaefer, III*

Center for Computational Quantum Chemistry, University of Georgia, Athens, Georgia 30602, United States

Supporting Information

ABSTRACT: The novel sandwich complex $Cp_2^*Al_2I_2$, which was recently synthesized by Minasian and Arnold, has been characterized using *ab initio* and density functional methods. A large family of related compounds was also investigated. Although a few Al(II)−Al(II) bonds are known, this is the first such bond to be supported by Cp-type ligands. In addition, in the remarkable $Cp_4^*Al_4$ synthesis by Roesky, $Cp_2^*Al_2I_2$ is the Al(II) intermediate; $Cp_4^*Al_4$ is important as a precursor to novel organoaluminum species. Halogen and ligand effects on the Al−Al bond in $Cp_2^*Al_2I_2$ were systematically explored by studying a series of 20 $Cp_2^*Al_2I_2$ derivatives using density functional theory with relativistic basis sets for the halogens. Comparison was made with the focal point treatment, which uses extrapolation to estimate the full configuration interaction and complete basis set limit energy. Torsional potential energy curves, natural population analyses, and enthalpies of hydrogenation were computed. Using the focal point approach, torsional barriers were computed with 0.05 kcal mol^{-1} uncertainty. The interplay of steric and electronic effects on the torsional potential energy curves, enthalpies of dehydrogenation reactions, and geometries is discussed. In species with small ligands (R = H, Me), hyperconjugative effects determine the torsional landscape, whereas steric repulsions dominate in species with Cp* alkyl ligands. Species with Cp ligands represent an intermediate case, thus providing insight into how ligands modulate the structures and properties of small metal clusters.

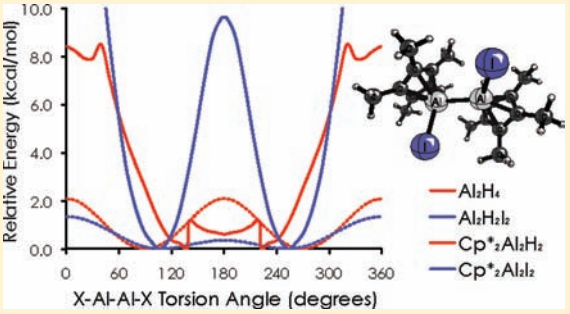

INTRODUCTION

The pentamethylcyclopentadienyl aluminum tetramer ($[Cp^*Al]_4$) was the first Al(I) compound found to be stable at room temperature.[1] The tetramer (Figure 1) features four aluminum atoms arranged in a tetrahedron, each of which is η^5 coordinated to a Cp* ring. $[Cp^*Al]_4$ has rich reactivity, so it is synthetically important as a precursor to aluminum-transition metal bonds,[2−5] aluminum−boron donor−acceptor bonds,[6] aluminum cluster complexes,[7] and iminoalanes.[8,9] In 1998, Schormann and co-workers reported a new synthetic route to $[Cp^*Al]_4$ which, unlike the original method, does not require extreme temperatures.[10] The reaction scheme is shown in Figure 2. This method involves reduction of an Al(III) compound ($[Cp^*AlI(\mu I)]_2$); in 2008 Minasian and Arnold isolated the Al(II) intermediate, $Cp_2^*Al_2I_2$.[11]

The current study was inspired by Minasian and Arnold's unusual Al(II) sandwich complex. Its crystal structure is shown in Figure 3. Homonuclear bonding in group 13 elements has attracted much attention,[12−14] particularly in the context of low oxidation state main group chemistry. Several of the known molecules with Al−Al bonds are formally aluminum(II), but none of them has Cp-type ligands.[15−19] Moreover, surprisingly little is known about divalent aluminum,[20] compared to its mono- and trivalent relatives.[21,22] Recent reviews highlight the importance of low oxidation state aluminum in modern inorganic chemistry. The aluminum(I) analogues of N-heterocyclic carbenes are precursors to exotic bicyclo and spiro organoaluminum species.[22] Low valent aluminum compounds have been proposed as intermediates in radical and photochemical reactions.[20] Many low oxidation state aluminum compounds have only lately become accessible, due to improved methods for handling these typically air-sensitive complexes.[20,21]

Molecules containing a nonmetallic Al−Al bond are called dialanes and are a recent synthetic achievement. The first dialane was made in 1988 by Werner Uhl.[23] The Al−Al bond is 2.66 Å long, surrounded by four bis(trimethylsilyl)methyl ligands. Rather bulky ligands are apparently required to support an Al−Al bond, since such ligands prevent disproportionation to aluminum metal[24] or polymerization.[25] Dialanes exhibit rich chemical reactivity, with Al−Al distances ranging from 2.5 to 2.9 Å. Thus, nonmetallic Al−Al bonds are generally shorter than the metallic Al−Al distance of 2.86 Å.[26] A few groups have succeeded in creating a one-electron π-bond in dialanes, typically in those containing large alkyl or silyl ligands.[15,27−32] The results are radical anions, with Al−Al bonds noticeably shorter than in the parent compounds. Wright and co-workers made a putative Al−Al double bond in 2003 but were unable to isolate it,[17] although it does undergo a Diels−Alder-type reaction with toluene. Three years later, the same group synthesized a compound with

Received: March 7, 2011
Published: June 26, 2011

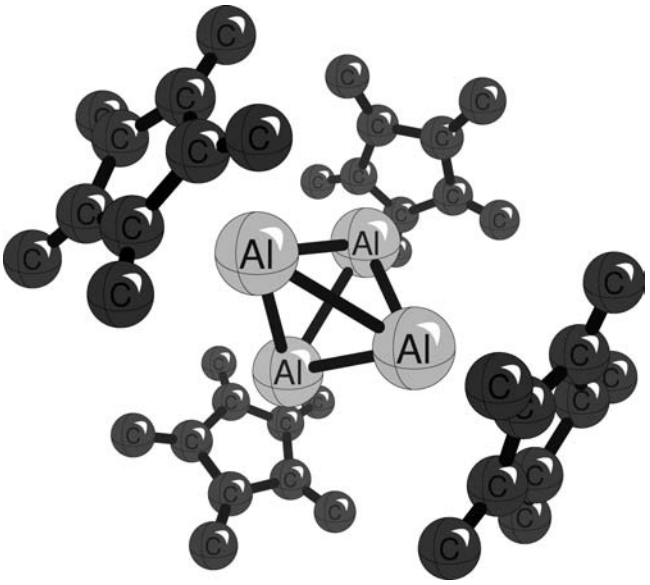

Figure 1. Crystal structure of Schnöckel and co-workers[1] for the pentamethylcyclopentadienyl aluminum(I) tetramer. Hydrogen atoms have been omitted for clarity.

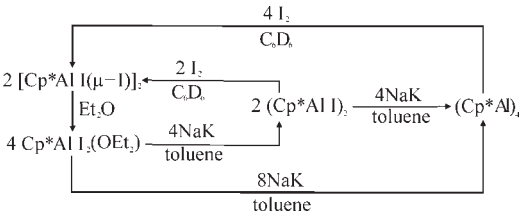

Figure 2. Experimental synthetic pathway to $[Cp^*Al]_4$ involving $Cp^*_2Al_2I_2$.[1]

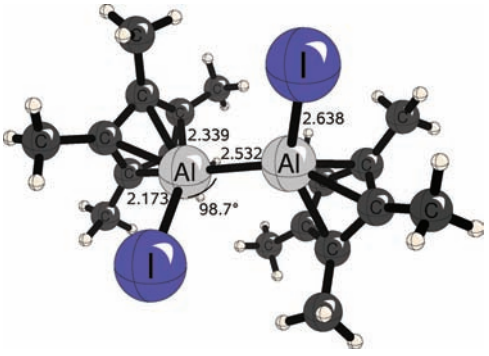

Figure 3. Crystal structure of Minasian and Arnold[11] for bispentamethylcyclopentadienyl diiododialane.

confirmed Al−Al multiple bonding and a compound containing a (possibly aromatic) Al_3 ring.[18] The subject of this study, $Cp^*_2Al_2I_2$, has an Al−Al distance of 2.52 Å and η^5 coordinated pentamethylcyclopentadienyl (Cp*) ligands.

Since 1991, several derivatives of $[Cp^*Al]_4$ have been synthesized. A variety of ligands can support the tetrahedral Al_4 core, including cyclopentadienyl (Cp) derivatives,[24,33] tBu$_3$SiAl,[34,35] $C(SiMe_3)_3$,[36] $Si(SiMe_3)_3$,[37] and 2,6-iPr$_2$C$_6$H$_3$N(SiMe$_3$).[38] A nearly tetrahedral Al_4 core can be supported solely by hydrogen atoms in the gas phase.[39] Substituted versions of Al_4H_6 have also been recently synthesized.[40] Uhl reviewed the structure and reactivity of Al_4 clusters in 2004,[41] noting their "particular bonding situation" and "aesthetic charm". The metal−metal bonding occurs through four highly delocalized molecular orbitals, formed from the lone-pair σ-orbitals of the monomers.[41] Only the cyclopentadienyl derivatives form π-bonds to aluminum; all others form σ-bonds.[22] Surprisingly, $Cp^*_4Al_4$ is stable to 140 °C, while Cp_4Al_4 decomposes at −50 °C.[24] The disproportionation of $Cp^*_4Al_4$ to metallic aluminum is hindered by a large barrier to formation of $Al_{50}Cp^*_{12}$,[42] the core of which resembles metallic aluminum packing.[43] However, if the Cp* ligands are replaced with Cp, there is almost no barrier to formation of the Al_{50} cluster. This significant change in physical properties due to methylation is not yet well understood.[24,42]

A number of organometallics containing clusters of aluminum atoms have been synthesized,[7,43−51] including the mixed aluminum and carbon clusters called carbaalanes.[49,50] Aluminum clusters are of interest since their cores resemble metallic packing and since they easily disproportionate to metallic aluminum.

Although large organometallics with Al−Al bonds are an important class of molecules, existing computational studies are limited. Several groups have performed computations on $[CpAl]_4$ and related species. Early studies investigated the bonding[34,52] and ^{27}Al NMR shifts[53] of AlX tetramers (X = H, F, Cl, Cp, SiH_3, $SiMe_3$, SitBu$_3$) at the SCF and MP2 levels of theory. When $[AlSitBu_3]_4$ was synthesized in 1998, experimental data were interpreted with the aid of DFT computations.[35] In 2008, the newly synthesized $[Al(C_5Me_4H)]_4$ was compared to $[Cp^*Al]_4$ and $[CpAl]_4$ using DFT results.[24] However, the remarkably disparate stabilities of $[Cp^*Al]_4$ and $[CpAl]_4$ mentioned above have yet to be explained.[24] Most recently, DFT computations were used to understand the bridged geometry of an Al−Al bond supported by phosphorus-based ligands (Al_2PtBu_4),[19,54] rather than a simple Al−Al bond between two R_2Al units.

The simplest dialane, Al_2H_4, has been the subject of in-depth computational studies. The global minimum for these six atoms is actually $AlH_4^-Al^+$ since aluminum is hypovalent,[55] and this arrangement best involves the formally unoccupied Al 3p$_z$-orbitals. However, $H_2Al-AlH_2$ is of interest as the aluminum analogue of ethylene and because it has been isolated in solid hydrogen matrices.[56,57] Molecular orbitals were computed,[58] and the global potential energy surface (PES) was explored[55,59,60] in early studies. More recently, Szabó and co-workers investigated why $X_2Al-AlX_2$ (X = H, F, Cl, Br, I) species prefer perpendicular (D_{2d}) geometries to planar (D_{2h}) structures.[61] It should be noted that, like Al_2H_4, the global minima for Al_2F_4 and Al_2Cl_4 are $AlX_4^-Al^+$,[54] although the $X_2Al-AlX_2$ geometry can be stabilized by donor groups.[21]

Interestingly, Al_2H_4 has the largest rotational barrier in the $X_2Al-AlX_2$ series, despite having the smallest ligands. At the TZ2P BP86 level of theory, it is 1.8 kcal mol^{-1}, which is about three times larger than the barriers for halogenated species.[61] This is consistent with Schleyer's analysis of the analogous boron compounds, H_2B-BH_2 and Cl_2B-BCl_2, based on the Hartree−Fock molecular orbitals.[62] First, B−H hyperconjugation is more effective than B−Cl hyperconjugation in the planar forms. Second, π conjugation of the halogen lone pairs into the empty boron p-orbitals is only present in Cl_2B-BCl_2. Taken together, these effects account for the fact that the torsional barrier of H_2B-BH_2 is 10.5 kcal mol^{-1}, while Cl_2B-BCl_2's is only 1.9 kcal mol^{-1}.[62] Szabó and co-workers came to similar

conclusions for Al compounds.[61] Thus, torsional analysis can give insight into the subtle interplay of steric and electronic effects.

In this study, we explore the torsional potential energy curves (PECs) of a series of dialanes, XRAl−AlRX (R = H, Me, Cp, Cp*: X = H, F, Cl, Br, I), initially using density functional theory (DFT). Natural bond orbital (NBO) reactivity descriptors, including charges and hyperconjugation strengths, are computed, which should guide future synthesis of novel small metal clusters. To benchmark the DFT results, we carry out focal point analyses with correlation treatments as extensive as CCSD(T) (coupled cluster, singles, doubles, and perturbative triples) and basis sets as large as aug-cc-pVQZ.

METHODS

Focal Point Analysis. Al_2H_4, $Al_2H_2F_2$, and $Al_2H_2Cl_2$ were characterized using coupled cluster singles and doubles (CCSD),[63−65] with perturbative triples (CCSD(T)),[66] in conjunction with augmented correlation-consistent polarized valence double, triple, and quadruple-ζ basis sets (aug-cc-pVDZ, aug-cc-pVTZ, and aug-cc-pVQZ).[67,68] Focal point tables were constructed according to the prescription of Allen.[69−72] The Hartree−Fock energy change (ΔE_{HF}) was extrapolated to the complete basis set (CBS) limit, using[73,74]

$$E_X = E_{CBS/HF} + (X + 1)be^{-9\sqrt{X}} \quad (1)$$

Here, X is the cardinal number of the basis set (e.g., $X = 2$ refers to the aug-cc-pVDZ basis set), while $E_{CBS/HF}$ and b are fitting coefficients. Next, the correlation energy is extrapolated to the CBS limit with[75]

$$E_X = E_{CBS}^{corr} + bX^{-3} \quad (2)$$

Again, E_{CBS}^{corr} and b are fitting coefficients. The energies and extrapolations are used to construct an incremented focal point table, in which the first column is the HF reaction energy and extrapolation to the CBS limit. Successive columns contain MP2, CCSD, and CCSD(T) corrections to the previous level of theory (e.g., $\delta[MP2] = \Delta E_{MP2} - \Delta E_{HF}$) and extrapolations to the CBS limit. Thus, the final column ($\Delta E_{CCSD(T)}$) is given by

$$\Delta E_{CCSD(T)} = \Delta E_{HF} + \delta[MP2] + \delta[CCSD] + \delta[CCSD(T)] \quad (3)$$

The final focal point estimate of the reaction energy (ΔE_{FP}) is found in the bottom right corner of the table and corresponds to an estimate of $\Delta E_{CCSD(T)}$ extrapolated to the CBS limit. Focal point analysis gives a detailed understanding of the reaction energy convergence, with respect to both increasing basis set size (columns) and correlation treatment (rows). In addition, examination of the table can yield an estimate of the error bars associated with the final reaction energy.

In these computations, only valence electrons are correlated. Corrections for core correlation were computed by taking the difference between frozen-core and all-electron MP2 single-point energies with cc-pCVTZ basis sets.[76−78]

Natural Bond Orbital Analysis. Natural population analyses were performed using the NBO 5.0 package and the B3LYP density functional in QChem.[79] DZP basis sets were employed for Al, C, and H, while DZVP basis sets[80]were used for the halogens since the NBO package in QChem is not compatible with partial use of pseudopotentials.

Computational Methods. $Cp_2^*Al_2I_2$, its derivatives, and its fragments were studied with density functional theory (DFT).[81] We used B3LYP[82,83] with DZP basis sets[84] for hydrogen, carbon, and aluminum. For iodine, the Stuttgart−Dresden−Bonn (SDB) pseudopotential and matching basis set[85] were selected to account for relativistic effects because an all-electron treatment was not feasible. SDB pseudopotentials and basis sets were selected for the smaller halogens to ensure consistent treatment. This computational approach is abbreviated DZP SDB B3LYP. A fine quadrature grid was employed, with 75 radial points and 302 angular. DFT and small basis CCSD(T) computations were carried out in the QChem 3.2 package.[86] Large basis CCSD(T) computations were performed with Molpro 2006.1.[87] The Natural Bond Orbital (NBO) 5.0 package was used for population analysis.[88−91]

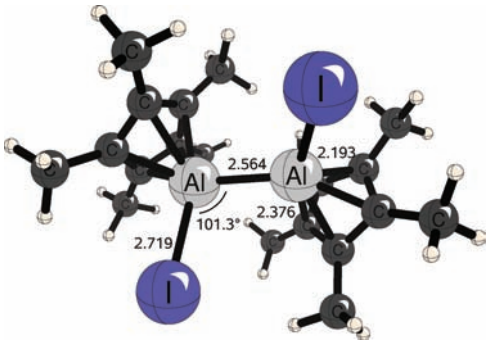

Figure 4. Theoretical geometry of Minasian and Arnold's compound[11] $Cp_2^*Al_2I_2$ at the DZP SDB B3LYP level of theory.

Table 1. Optimized Structural Parameters for $Cp_2^*Al_2I_2$ and Several Related Complexes[a]

structure	halogen	r(Al−Al)	r(Al−X)	τ(X−Al−Al−X)	r(Al−ligand)	hapticity
$Cp_2^*Al_2X_2$	H	2.527	1.607	137.8	2.136−3.002	2
	F	2.537	1.731	166.1	2.178−2.376	5
	Cl	2.549	2.266	120.7	2.169−2.420	5
	Br	2.560	2.447	113.4	2.177−2.405	5
	I	2.564	2.719	107.0	2.184−2.375	5
$Cp_2Al_2X_2$	H	2.518	1.594	127.7	2.155−3.106	2
	F	2.492	1.700	138.4	2.129−2.880	2
	Cl	2.499	2.185	116.9	2.121−2.909	2
	Br	2.506	2.342	112.7	2.125−2.917	2
	I	2.508	2.584	110.7	2.123−2.916	2
$Me_2Al_2X_2$	H	2.596	1.596	92.0	1.970	
	F	2.585	1.694	180.0	1.947	
	Cl	2.580	2.166	160.0	1.947	
	Br	2.578	2.317	138.4	1.950	
	I	2.568	2.549	120.1	1.951	
$H_2Al_2X_2$	H	2.579	1.589	90.1	1.589	
	F	2.575	1.687	112.1	1.577	
	Cl	2.569	2.152	109.9	1.575	
	Br	2.568	2.299	110.2	1.576	
	I	2.561	2.525	109.8	1.576	

[a] Structural parameters are in Å and degrees. The Al−ligand distances are measured to ring-carbon atoms for Cp groups and to the appropriate carbon atom for methyl groups.

RESULTS AND DISCUSSION

Geometric Structures. Comparison of computed geometries with experimental measurements provides an important benchmark for the theoretical methods employed. The minimum energy structure of $Cp_2^*Al_2I_2$ at the DZP SDB B3LYP level is in good agreement with the crystal structure; it is shown in Figure 4. The Al−Al distance of 2.56 Å agrees with the measured bond length of 2.53 Å, and the Cp* rings are η^5 coordinated. The theoretical carbon to aluminum distances range from 2.18 to 2.38 Å around the ring, which compares very favorably with the experimental range of 2.17−2.34 Å. The Al−I distance is 2.72 Å

Table 2. Out-of-Plane Al $3p_z$ Atomic Orbital Populations (e) for C_{2h} Geometries of Selected Dialanes at the DZVP B3LYP Level of Theory

	ligand	
halogen	H	Me
H	0.001	0.018
F	0.061	0.070
Cl	0.093	0.102
Br	0.107	0.114
I	0.127	0.132

at the DZP SDB B3LYP level of theory, while the measured value is 2.64 Å. However, the I−Al−Al−I torsional angle in the optimized structure is 107°, which disagrees with the crystal structure value of 91°. To resolve this point, the torsional PEC about the Al−Al bond was explored. The I−Al−Al−I dihedral angle was varied in 10° increments from the equilibrium value, and all other structural parameters were allowed to relax. Changing the torsion angle to 90° only raises the energy by about 0.5 kcal mol^{-1}. This shallow torsional potential energy curve and possible crystal packing effects resolve the apparent disagreement with experiment. Thus, where crystal structures are available, good agreement with experiment should be achieved.

We investigated halogen and ligand effects on $Cp^*_2Al_2I_2$ by replacing the iodine atoms with bromine, chlorine, fluorine, or hydrogen atoms and the Cp* ligand with Cp, Me, or H. Each structure was independently optimized, and harmonic vibrational frequencies were computed to identify stationary points as minimum energy structures. The reported geometric parameters are for minimum energy geometries (see Table 1 for a summary of the results). All of the structures considered here are closed-shell singlets, with HOMO−LUMO gaps of at least 4 eV.

If the alkyl ligand is H or Me, the Al−Al bond length decreases with increasing weight of X, from 2.579 Å in Al_2H_4 to 2.561 Å in $Al_2H_2I_2$ and from 2.596 Å in $Al_2Me_2H_2$ to 2.568 Å in $Al_2Me_2I_2$. The less electronegative larger halogens donate electrons to the empty 3p orbital on aluminum. This can be seen in the natural populations of the aluminum $3p_z$ orbital, shown in Table 2. Note that all species are in C_{2h} symmetry for this analysis, to make the axes and orbitals unambiguously identifiable. The occupation of this formally empty $3p_z$ orbital increases steadily with increasing halogen size, increasing the double bond character of the Al−Al interaction and shortening the bond.

However, the bond length ordering changes significantly with larger alkyl ligands. In the Cp series, the Al−Al distance increases with increasing halogen weight, from fluorine (2.492 Å) to iodine (2.508 Å). Hydrogen-substituted $Cp_2Al_2H_2$ has the longest Al−Al distance in the series (2.518 Å). The trend becomes clear in the Cp* series; the Al−Al distance increases from 2.527 Å in $Cp^*_2Al_2H_2$ to 2.564 Å in $Cp^*_2Al_2I_2$. A graphical summary of these trends is presented in Figure 5.

Torsional PECs were computed for all structures by varying the X−Al−Al−X dihedral angle in 10° increments and allowing all other parameters to relax. These are displayed in Figure 6 through Figure 9. We find the largest torsional barriers in $H_2Al_2X_2$ and $Me_2Al_2X_2$ for X = H. If X is a halogen, the PEC

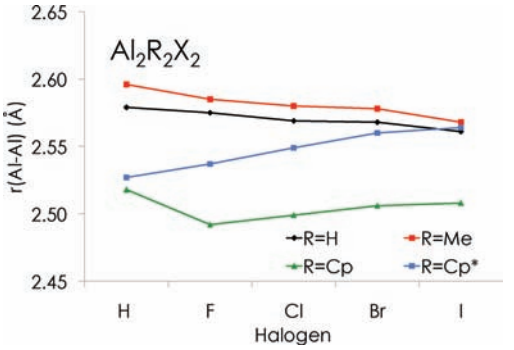

Figure 5. Al−Al distance plotted against halogen substituent in aluminum dimetallocenes at the DZP SDB B3LYP level of theory.

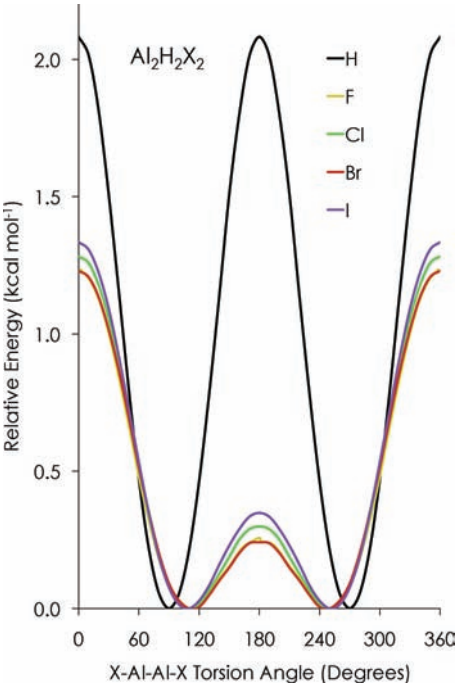

Figure 6. Torsional potential energy curves for $Al_2H_2X_2$ at the DZP SDB B3LYP level of theory.

is very flat between 110° and 250°, changing by less than 0.35 kcal mol^{-1} for $H_2Al_2X_2$ and less than 0.10 kcal mol^{-1} for $Me_2Al_2X_2$. By way of illustration, Al_2H_4 has a barrier of 2.0 kcal mol^{-1}, versus only 0.3 kcal mol^{-1} for $Al_2H_2I_2$. Similarly, $Me_2Al_2H_2$'s barrier is 1.0 kcal mol^{-1}, versus 0.1 kcal mol^{-1} for the iodine version. This is in line with previous work on Al_2X_4 species.[61] The large barriers for hydrogen-substituted dialanes are due to hyperconjugation in the twisted geometry and the absence of conjugations or hyperconjugations in the planar form. The barriers decrease when X is a halogen because the lone pairs overlap favorably with the empty Al $3p_z$ orbital in the planar form, as shown in Table 2 and discussed below. This offsets the loss of hyperconjugation, lowers the internal rotational barrier,[61] and explains the nonintuitive ordering of barrier heights in $H_2Al_2X_2$ and $Me_2Al_2X_2$.

Interestingly, the rotational barriers in $Cp^*_2Al_2X_2$ and $Cp_2Al_2X_2$ generally increase with the mass of the halogen, while hydrogen falls between fluorine and chlorine. The largest barrier in each series

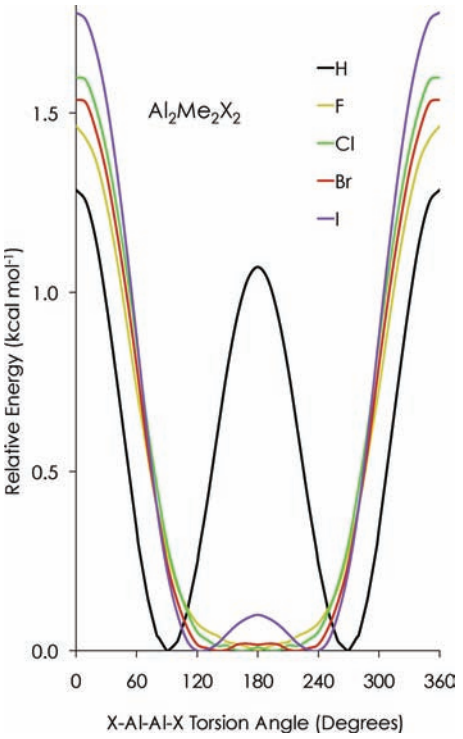

Figure 7. Torsional potential energy curves for $Al_2Me_2X_2$ at the DZP SDB B3LYP level of theory.

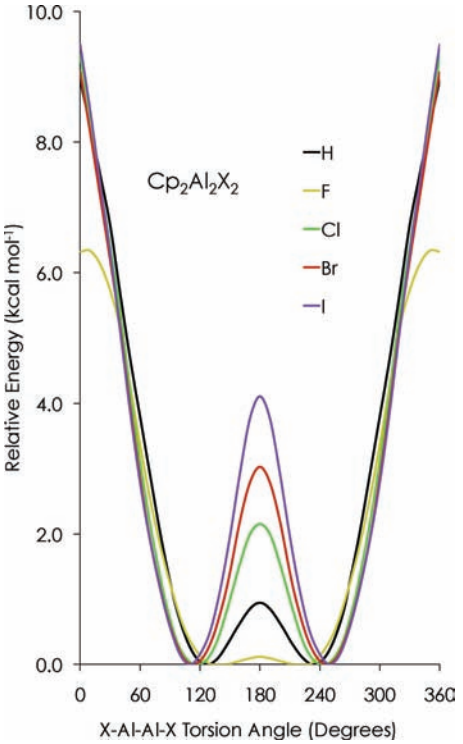

Figure 8. Torsional potential energy curves for $Cp_2Al_2X_2$ at the DZP SDB B3LYP level of theory.

corresponds to iodine: $Cp_2Al_2I_2$ (4 kcal mol^{-1}) and $Cp^*_2Al_2I_2$ (10 kcal mol^{-1}). Torsional barriers are plotted against the halogen substituent in Figure 10. Although the general trends seen in the

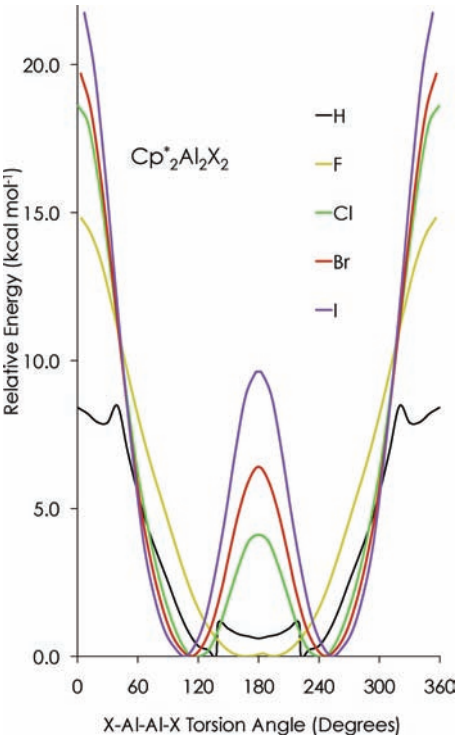

Figure 9. Torsional potential energy curves for $Cp^*_2Al_2X_2$ at the DZP SDB B3LYP level of theory.

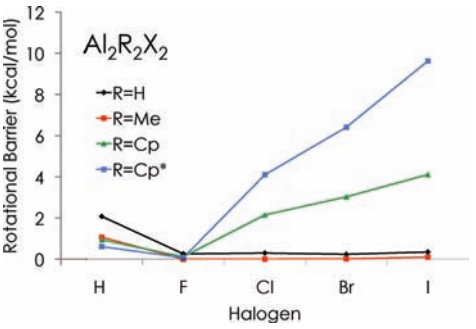

Figure 10. Al—Al torsional barrier plotted against halogen substituent in aluminum dimetallocenes at the DZP SDB B3LYP level of theory.

small alkyl substituents reverse with Cp and Cp* species, those with fluorine consistently have smaller rotational barriers than those with hydrogen. Thus, even in large molecules, hyperconjugation seems to determine the ordering of the rotational barriers for the fluorine- and hydrogen-substituted systems. As seen in Table 3, the Al—Al bond lengthens more with larger alkyl groups and larger halogens. This may indicate that steric effects are more significant than hyperconjugation when large alkyl groups and heavy halogens are present. Further evidence for this explanation is given in Figure 11. Here, the population of the $3p_z$ orbital on aluminum is plotted against halogen substituent for all four series of alkyl ligands. The formally empty $3p_z$ orbital on aluminum was identified as the formally unoccupied lone-pair (LP*) natural bond orbital with the largest p-character (over 90%) and largest population. Since NBO assigns two-center bonds, it gives an incomplete description of aromatic rings like Cp. Thus, it assigned as many as three partially occupied non-Lewis orbitals with some $3p_z$ character

dx.doi.org/10.1021/ja2020845 |J. Am. Chem. Soc. 2011, 133, 13387–13396

Table 3. Lengthening of the Al−Al Bond during Torsion from Equilibrium to τ(X−Al−Al−X) = 180°

	ligand			
halogen	H	Me	Cp	Cp*
H	1.05%	0.85%	0.68%	1.62%
F	0.19%	0.00%	0.52%	0.16%
Cl	0.31%	0.04%	1.60%	2.39%
Br	0.31%	0.16%	1.84%	3.13%
I	0.43%	0.39%	2.31%	4.33%

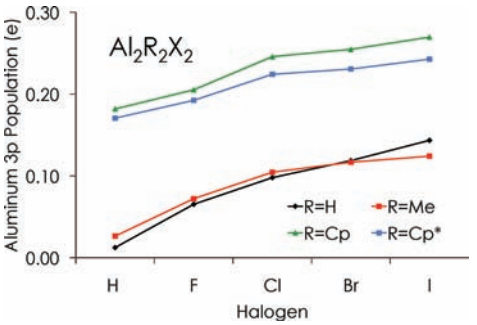

Figure 11. Aluminum lone-pair 3p NBO populations at the DZVP B3LYP level of theory.

to aluminum in the Cp and Cp* series. This is not a significant problem since we are primarily interested in the Al−Al bond. Figure 11 clearly shows that the larger halogens are better donors to the empty $3p_z$ orbital on aluminum. However, competing steric effects cause the trends followed in the small species to reverse in species with Cp and Cp* alkyl ligands.

While most of the potential curves are smooth, the PEC for $Cp^*_2Al_2H_2$ oscillates. The bumps correspond to abrupt changes in the Cp* hapticity. $Cp^*_2Al_2H_2$ has η^5 hapticity below 30° and between 140° and 180°. Between 40° and 130°, it is η^2. This is evidenced by sharp changes in the range of Al−C_{ring} distances, while the Al−Al and Al−H distances are essentially unchanged. In general, Cp* rings have higher hapticity than Cp rings, evidenced by narrower ranges of ring-carbon to aluminum distances (Table 1). The hapticity also increases with increasing halogen size; for example, the Cp* hapticity increases from two in $Cp^*_2Al_2H_2$ to five in $Cp^*_2Al_2I_2$. Consistent with these two trends, $Cp^*_2Al_2I_2$ has the narrowest range of ring-carbon to aluminum distances (2.184−2.375 Å), while $Cp_2Al_2H_2$ has the largest range (2.155−3.106 Å).

To estimate the Al−Al bond strength, 0 K enthalpies of dehydrogenation of hydrogen-capped monomers were computed using harmonic zero-point energies. The monomers' geometries were optimized independently, and the changes in enthalpy were computed for the following reactions

$$2H_2AlX \rightarrow H_2Al_2X_2 + H_2$$

$$2MeAlHX \rightarrow Me_2Al_2X_2 + H_2$$

$$2Cp^*AlHX \rightarrow Cp^*_2Al_2X_2 + H_2$$

$$2CpAlHX \rightarrow Cp_2Al_2X_2 + H_2$$

The dehydrogenation enthalpy results are summarized in Table 4 and Figure 12. Examination of the results for alkyl

Table 4. 0 K Enthalpies of Dehydrogenation for Al−Al Species from Hydrogen-Capped Monomers at the DZP SDB B3LYP Level

structure	halogen	ΔH_{rxn} (kcal mol^{-1})	r(Al−Al) (Å)	hapticity
$Cp^*_2Al_2X_2$	H	+6.4	2.527	2
	F	−2.1	2.537	5
	Cl	+0.1	2.549	5
	Br	+0.9	2.560	5
	I	+1.0	2.564	5
$Cp_2Al_2X_2$	H	+1.2	2.518	2
	F	−2.5	2.492	2
	Cl	−2.6	2.499	2
	Br	−2.5	2.506	2
	I	−3.1	2.508	2
$Me_2Al_2X_2$	H	+7.7	2.596	
	F	+4.4	2.585	
	Cl	+3.5	2.580	
	Br	+3.2	2.578	
	I	+1.9	2.568	
$H_2Al_2X_2$	H	+6.3	2.579	
	F	+5.5	2.575	
	Cl	+4.6	2.569	
	Br	+3.8	2.568	
	I	+2.5	2.561	

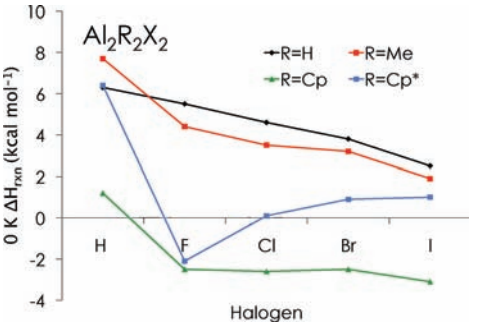

Figure 12. Dehydrogenation reaction enthalpy plotted against halogen substituent in aluminum dimetallocenes at the DZP SDB B3LYP level of theory.

ligands H and Me reveals that the shorter Al−Al bonds correspond to larger dehydrogenation energies. In both series, the Al−Al distance decreases down the series, and the ΔH_{rxn} also decreases. This trend is not followed in the Cp series; the enthalpies of dehydrogenation for F, Cl, Br, and I substituted species are all nearly −3 kcal mol^{-1}. However, the hydrogen-substituted version has a +1 kcal mol^{-1} enthalpy of dehydrogenation. The picture is somewhat clearer in the Cp* series; with the exception of the H-substituted species, the enthalpy of dehydrogenation increases with lengthening bond distance. $Cp^*_2Al_2H_2$ does not fit the trend since it has η^2 Cp* rings, while the others have η^5 ligands. Thus, as in the discussions of Al−Al distances and rotational barriers, the Cp series represents the crossover from electronic effects dominating in the small alkyl ligands (H, Me) to steric effects, which dominate in the Cp* series. A graphical summary is presented in Figure 12.

dx.doi.org/10.1021/ja2020845 |J. Am. Chem. Soc. 2011, 133, 13387–13396

NBO DESCRIPTORS

The NBO donor−acceptor paradigm provides a powerful conceptual framework for understanding the subtle hyperconjugative effects in Al_2X_4 species, particularly those involving the formally unoccupied $3p_z$ orbitals on Al. NBO quantifies qualitative bonding concepts, such as hyperconjugation, charge transfer, and other donor−acceptor interactions, including dative coordination. This approach reveals why DFT methods overestimate the torsional barrier in Al_2H_4 compared to highly accurate correlated methods (see next section). The atomic $3p_z$ population on aluminum was computed at various levels of theory, both at the flat D_{2h} and twisted D_2 DZP B3LYP geometries. With each method shown in Table 11 the $3p_z$ populations are very similar at the D_{2h} geometry. However, both B3LYP and BP86 are overly delocalized at the D_2 geometry. The extent to which DFT functionals overestimate the torsional barrier is closely related to how much they overestimate the $3p_z$ population at the D_2 geometry, compared with the aug-cc-pVTZ HF result. Although the population differences are rather small, delocalization is a strong energy lowering effect and could certainly account for the difference in barrier heights. The extra delocalization in the DFT results (amounting to about 0.005 electrons per aluminum atom and 0.01 electrons total) could account for up to a 6 kcal mol^{-1} difference in the barrier heights.

The energy lowering (ΔE) due to mixing an occupied orbital (ϕ_i) with an unoccupied orbital (ϕ_{j^*}) can be calculated using second-order perturbation theory. In NBO terms, ϕ_i and ϕ_{j^*} are rigorously localized one- or two-center orbitals, and ΔE describes the energy benefit of their mixing to form a rigorously doubly occupied orbital. F_{i,j^*} is the Fock matrix element between the two orbitals, and ε_i and ε_{j^*} are the respective orbital energies.[92]

$$\Delta E = 2\frac{F_{i,j*}^2}{\varepsilon_i - \varepsilon_{j*}} \quad (4)$$

The number of electrons (q) transferred from ϕ_i to ϕ_{j^*} can be approximated by

$$q = 2\frac{F_{i,j*}^2}{(\varepsilon_i - \varepsilon_{j*})^2} \quad (5)$$

An approximation for the energy lowering due to orbital mixing/charge transfer is given by[93,94]

$$q \times (\varepsilon_i - \varepsilon_{j*}) = \Delta E \quad (6)$$

The orbital energy differences involved are on the order of 1 hartree; in the $Al_2H_2X_2$ series the orbital energy difference between the lone pairs on the halogen and the formally empty 3p orbital on aluminum range from 0.27 au (X = Cl) to 0.93 au (X = Br). In the largest system, $Cp^*_2Al_2I_2$, the lone pairs on iodine are 0.97 au lower in energy than the empty 3p orbital on aluminum. Thus, the above equation can be further approximated as

$$q \approx \Delta E \quad (7)$$

In this equation, q is the number of electrons and ΔE is in Hartrees. (These equations assume that the orbitals mix to a small extent, and thus the original orbitals are not strongly perturbed by the interaction.) Thus, the transfer of 0.01 electrons is worth about 6 kcal mol^{-1}. From Table 11, this extra delocalization is not isolated to the B3LYP functional.

Table 5. Halogen Natural Charges at the DZVP B3LYP Level of Theory

	ligand			
structure	H	Me	Cp	Cp*
$Al_2R_2H_2$	−0.37	−0.39	−0.38	−0.40
$Al_2R_2F_2$	−0.75	−0.76	−0.75	−0.76
$Al_2R_2Cl_2$	−0.55	−0.56	−0.55	−0.58
$Al_2R_2Br_2$	−0.47	−0.49	−0.47	−0.52
$Al_2R_2I_2$	−0.35	−0.38	−0.35	−0.43

Table 6. Aluminum Natural Charges at the DZVP B3LYP Level of Theory

	ligand			
halogen	H	Me	Cp	Cp*
H	0.73	0.98	0.94	1.00
F	1.16	1.37	1.33	1.40
Cl	0.92	1.14	1.08	1.17
Br	0.84	1.07	1.00	1.11
I	0.70	0.94	0.87	1.00

The energy lowering due to delocalization can be further dissected into contributions from particular bonds; this is found in the E2PERT table of the NBO output. In twisted Al_2H_4 at the DZP B3LYP level, each Al−H bond hyperconjugates with the formally empty 3p orbital on the neighboring aluminum atom. Each interaction is worth about 1.34 kcal mol^{-1}, for a total of 5.36 kcal mol^{-1}. This is reasonably similar to the above estimate of 6 kcal mol^{-1}. The Al−H to 3p hyperconjugation is absent in planar Al_2H_4, and since it occurs across the Al−Al bond in twisted Al_2H_4, it contributes to the torsional barrier.

Similar reasoning can be applied to the torsional barrier in $Al_2H_2F_2$, which is +0.26 kcal mol^{-1} at the DZP SDB B3LYP level of theory but less than 1 cm^{-1} using cc-pVDZ CCSD(T) geometries and energies (see next section). Examination of the NBO output at the DZVP B3LYP level reveals that hyperconjugation is greatly reduced in $Al_2H_2F_2$, due to the very polarized Al−F bonds. In both the planar and twisted geometries, donation from the Al−F bond to 3p on the neighboring aluminum is worth less than 0.10 kcal mol^{-1} and does not appear in the NBO output. Lone pairs on fluorine interact significantly with the 3p orbital on the closest aluminum atom. However, this vicinal conjugation is virtually unaffected by twisting the molecule and thus does not contribute to the rotational barrier. Two kinds of delocalization occur in twisted $Al_2H_2F_2$ which are absent in the planar form. There is a slight donation (0.13 kcal mol^{-1}) from a fluorine lone pair to the opposite aluminum 3p orbital. Finally, donation from the Al−H bond is significantly reduced, compared to Al_2H_4; each interaction is worth only 0.63 kcal mol^{-1}. The above discussion of Al_2H_4 indicates that B3LYP tends to overestimate delocalizations, so it is not unreasonable that the very small rotational barrier in $Al_2H_2F_2$ disappears with the more accurate CCSD(T) method. This possibly warrants further investigation. However, we demonstrated above that B3LYP reproduces trends for these systems and is a suitable level of theory for this study; although the rotational barriers tend to be overestimated, the trends are reproduced correctly.

The natural charges on the halogen atoms were consistent over all the structures (see Table 5). The natural charge residing on aluminum is shown in Table 6. It is evident that characterizing $Cp^*_2Al_2I_2$ as an Al(II) complex is somewhat misleading. Since Al is less electronegative than C, H, or any halogen, all ligands are formally assigned a −1 charge, leaving Al with a formal +2 charge. However, the ligand natural charges are all closer to −0.5 than to −1 (Table 7). The natural charge on aluminum is only +1 in $Cp^*_2Al_2I_2$ and not larger than +1.4 in any of the molecules considered. The ligands participate in donor−acceptor interactions with the $3p_z$ orbital on Al, preventing a large natural charge from accumulating on the metal atoms.

Focal Point Analysis and Structural Benchmarks. To evaluate the reliability of the B3LYP treatments, energies, structural parameters, and harmonic vibrational frequencies were computed for the parent Al_2H_4 and its dissociation to AlH_2. (Full results are provided in the Supporting Information.) In general, B3LYP is in excellent agreement with CCSD(T) for these systems, with bond lengths within 0.02 Å, angles within 0.6°, and frequencies within 18 cm^{-1}. There are a few notable exceptions; the B3LYP dissociation energy for Al_2H_4 is 4.2 kcal mol^{-1} too low, and the torsional mode (ν_1) for Al_2H_4 is overestimated by about 40% (46 cm^{-1}) at the DZP B3LYP level of theory. Finally, the rotational barrier is 1 kcal mol^{-1} too high. A previous study on ethane and its analogues (C_2H_6, Si_2H_6, $SiGeH_6$, and Ge_2H_6) found that B3LYP underestimates their rotational barriers by about 10%, while CCSD(T) may overestimate them.[95] However, focal point analysis of the Al_2H_4 barrier (Table 8) indicates that the CCSD(T) estimate is well converged with respect to theory and basis set. The CCSD(T) increment is 0.07 kcal mol^{-1}. Subsequent corrections are expected to be much smaller since quadruple excitations contribute less than triple excitations. Changing the basis set from aug-cc-pVTZ to aug-cc-pVQZ only changes the CCSD and CCSD(T) increments by 0.01 kcal mol^{-1}, indicating that cc-pVQZ is a close approximation to the CBS limit for this system. Thus, the uncertainty in the final estimate (ΔE_{FP}) is on the order of 0.05 kcal mol^{-1}. B3LYP overestimates the torsional barrier in this molecule. Physical reasons for this are discussed below.

Focal point tables were also computed for the torsional barriers in $Al_2H_2F_2$, $Al_2H_2Cl_2$, and $Al_2H_2Br_2$. The rotational barriers converged very quickly, with respect to both correlation and basis set. The uncertainty is on the order of 0.05 kcal mol^{-1}. Core corrections to the rotational barriers were found to be negligible. These results are compared to the DZP B3LYP barriers in Table 9, and full focal point tables are provided in the Supporting Information. Physical insight into why DFT overestimates the torsional barrier in $Al_2H_2F_2$ is provided by NBO analysis. (See next section.)

To further benchmark the DFT results, we carried out focal point analysis on the following reactions

$$2AlH_3 \rightarrow Al_2H_4 + H_2$$

$$2AlH_2F \rightarrow Al_2H_2F_2 + H_2$$

$$2AlH_2Cl \rightarrow Al_2H_2Cl_2 + H_2$$

$$2AlH_2Br \rightarrow Al_2H_2Br_2 + H_2$$

Table 7. Ligand Natural Charges at the DZVP B3LYP Level of Theory Computed as the Difference Between the NPA of Aluminum and That of the Halogen

	ligand			
halogen	H	Me	Cp	Cp*
H	−0.37	−0.59	−0.56	−0.60
F	−0.41	−0.61	−0.58	−0.64
Cl	−0.37	−0.58	−0.53	−0.59
Br	−0.36	−0.58	−0.53	−0.59
I	−0.35	−0.57	−0.51	−0.57

Table 9. Comparison of DFT Torsional Barriers (kcal mol^{-1}) in $Al_2H_2X_2$ Species to Focal Point Results

halogen	focal point barrier	DZP SDB B3LYP barrier
H	+1.03[a]	+2.08
F	<0.01[b]	+0.26
Cl	+0.13[a]	+0.30
Br	+0.23[a]	+0.24

[a] DZP SDB B3LYP geometries. [b] cc-pVDZ CCSD(T) geometries. See Supporting Information.

Table 10. Comparison of Focal Point Reaction Energies (kcal mol^{-1}) of $2AlH_2X \rightarrow Al_2H_2X_2 + H_2$ to DFT Results

halogen	core corrected focal point ΔE_{rxn}	DZP B3LYP ΔE_{rxn}
H	+3.55	+7.1
F	+4.42	+6.7
Cl	+2.79	+5.8
Br	+1.88	+5.0

Table 11. Aluminum 3p Populations and Rotational Barriers for Al_2H_4

	level of theory			
property	aug-cc-pVTZ HF	DZP HF	DZP B3LYP	DZP BP86
D_{2h} 3p occ.	0.0008	0.0007	0.0007	0.0007
D_2 3p occ.	0.0045	0.0058	0.0123	0.0170
barrier (kcal mol^{-1})	0.88	1.59	2.08	2.38

Table 8. Focal Point Analysis of the Torsional Barrier[a] for Al_2H_4 in kcal mol^{-1}

	ΔE_{HF}	+δ[MP2]	+δ[CCSD]	+δ[CCSD(T)]	$\Delta E_{CCSD(T)}$
aug-cc-pVDZ	+0.81	+0.21	−0.05	+0.05	[+1.02]
aug-cc-pVTZ	+0.88	+0.23	−0.08	+0.06	[+1.09]
aug-cc-pVQZ	+0.84	+0.21	−0.07	+0.07	[+1.04]
CBS LIMIT	[+0.84]	[+0.19]	[−0.07]	[+0.07]	[+1.03]
fit	$a + (X+1)be^{-9(X)^{1/2}}$	$a + bX^{-3}$	$a + bX^{-3}$	$a + bX^{-3}$	

[a] Energies were computed at DZP B3LYP geometries.

The core-corrected focal point reaction energies are compared to DFT results in Table 10; full focal point tables are provided in the Supporting Information. The reaction energies converged more slowly to the CBS FCI limit than the torsional barriers did, and the uncertainty in the final ΔE_{FP} is approximately 0.5 kcal mol^{-1}. Although DZP SDB B3LYP overestimates the torsional barriers and reaction energies, the trends are reproduced correctly. These results indicate that DZP B3LYP is a suitable level of theory for a qualitative study of Al−Al bonding. While CCSD(T) is the "gold-standard" for computational chemistry, B3LYP is currently a necessity for large systems like $Cp^*_2Al_2I_2$.

CONCLUDING REMARKS

We have completed a systematic study of aluminum dimetallocenes using *ab initio* and density functional methods. This is an exciting new class of organoaluminum molecules, the first of which ($Cp^*_2Al_2I_2$) was recently synthesized by Minasian and Arnold. Electronic effects, such as hyperconjugation, were found to be crucial in the small $Al_2R_2X_2$ (R = H, Me) species. NBO analysis shows clear relationships between hyperconjugative interactions, torsional barrier heights, and Al−Al bond lengths. However, these trends are reversed in species with Cp* ligands, with Cp being an intermediate case. NBO analysis is especially useful in this regard because it connects electronic structure theory to a chemically intuitive picture of bonding. This research should provide deeper insight into novel aluminum organometallics, provide computational benchmarks for such molecules, and guide future synthesis efforts.

ASSOCIATED CONTENT

Supporting Information. Complete data tables, coordinates, and energies for optimized structures and complete references 86 and 87. This material is available free of charge via the Internet at http://pubs.acs.org.

AUTHOR INFORMATION

Corresponding Author
fri@uga.edu

ACKNOWLEDGMENT

This research was supported by the U.S. National Science Foundation, Grant CHE-1054286. The authors thank Andy Simmonett, Lucas Speakman, and Francesco Evangelista for helpful discussions.

REFERENCES

(1) Dohmeier, C.; Robl, C.; Tacke, M.; Schnöckel, H. *Angew. Chem., Int. Ed. Engl.* **1991**, *30*, 564–565.
(2) Üffing, C.; Ecker, A.; Köppe, R.; Schnöckel, H. *Organometallics* **1998**, *17*, 2373–2375.
(3) von Hänisch, C. K. F.; Üffing, C.; Junker, M. A.; Ecker, A.; Kneisel, B. O.; Schnöckel, H. *Angew. Chem., Int. Ed. Engl.* **1996**, *35*, 2875–2877.
(4) Schulz, S.; Schoop, T.; Roesky, H. W.; Häming, L.; Steiner, A.; Herbst-Irmer, R. *Angew. Chem., Int. Ed. Engl.* **1995**, *34*, 919–920.
(5) Dohmeier, C.; Krautscheid, H.; Schnöckel, H. *Angew. Chem., Int. Ed. Engl.* **1994**, *33*, 2482–2483.
(6) Gorden, J. D.; Voigt, A.; Macdonald, C. L. B.; Silverman, J. D.; Cowley, A. H. *J. Am. Chem. Soc.* **2000**, *122*, 950–951.
(7) Purath, A.; Dohmeier, C.; Ecker, A.; Köppe, R.; Krautscheid, H.; Schnöckel, H.; Ahlrichs, R.; Stoermer, C.; Friedrich, J.; Jutzi, P. *J. Am. Chem. Soc.* **2000**, *122*, 6955–6959.
(8) Timoshkin, A. Y. *Coord. Chem. Rev.* **2005**, *249*, 2094–2131.
(9) Schulz, S.; Häming, L.; Herbst-Irmer, R.; Roesky, H. W.; Sheldrick, G. M. *Angew. Chem., Int. Ed. Engl.* **1994**, *33*, 969–970.
(10) Schormann, M.; Klimek, K. S.; Hatop, H.; Varkey, S. P.; Roesky, H. W.; Lehmann, C.; Röpken, C.; Herbst-Irmer, R.; Noltemeyer, M. *J. Solid State Chem.* **2001**, *624*, 513–516.
(11) Minasian, S. G.; Arnold, J. *Chem. Commun.* **2008**, 4043–4045.
(12) Xie, Y.; Grev, R. S.; Gu, J.; Schaefer, H. F.; von Ragué Schleyer, P.; Su, J.; Li, X.-W.; Robinson, G. H. *J. Am. Chem. Soc.* **1998**, *120*, 3773–3780.
(13) Wang, Y.; Quillian, B.; Wei, P.; Wannere, C. S.; Xie, Y.; King, R. B.; Schaefer, H. F.; von Ragué Schleyer, P.; Robinson, G. H. *J. Am. Chem. Soc.* **2007**, *129*, 12412–12413.
(14) Quillian, B.; Wei, P.; Wannere, C. S.; von Ragué Schleyer, P.; Robinson, G. H. *J. Am. Chem. Soc.* **2009**, *131*, 3168–3169.
(15) Wehmschulte, R. J.; Ruhlandt-Senge, K.; Olmstead, M. M.; Hope, H.; Sturgeon, B. E.; Power, P. P. *Inorg. Chem.* **1993**, *32*, 2983–2984.
(16) Wiberg, N.; Amelunxen, K.; Blank, T.; Nöth, H.; Knizek, J. *Organometallics* **1998**, *17*, 5431–5433.
(17) Wright, R. J.; Phillips, A. D.; Power, P. P. *J. Am. Chem. Soc.* **2003**, *125*, 10784–10785.
(18) Wright, R. J.; Brynda, M.; Power, P. P. *Angew. Chem., Int. Ed.* **2006**, *45*, 5953–5956.
(19) Henke, P.; Pankewitz, T.; Klopper, W.; Breher, F.; Schnöckel, H. *Angew. Chem., Int. Ed.* **2009**, *48*, 8141–8145.
(20) Rao, M. N. S.; Roesky, H. W.; Anantharaman, G. *J. Organomet. Chem.* **2002**, *646*, 4–14.
(21) Dohmeier, C.; Loos, D.; Schnöckel, H. *Angew. Chem., Int. Ed. Engl.* **1996**, *35*, 129–149.
(22) Nagendran, S.; Roesky, H. W. *Organometallics* **2008**, *27*, 457–492.
(23) Uhl, W. *Z. Naturforsch.* **1988**, *43b*, 1113–1118.
(24) Huber, M.; Schnöckel, H. *Inorg. Chim. Acta* **2008**, *361*, 457–461.
(25) Turley, J. W.; Rinn, H. W. *Inorg. Chem.* **1969**, *8*, 18–22.
(26) *CRC Handbook of Chemistry and Physics*, 88th ed.; Lide, D. R., Ed.; CRC Press: Boca Raton, FL 33487, 2008.
(27) Uhl, W.; Vester, A.; Kaim, W.; Poppe, J. *J. Organomet. Chem.* **1993**, *454*, 9–13.
(28) Pluta, C.; Pörschke, K.-R.; Krüger, C.; Hildenbrand, K. *Angew. Chem., Int. Ed. Engl.* **1993**, *32*, 388–390.
(29) Wang, Y.; Robinson, G. H. *Organometallics* **2007**, *26*, 2–11.
(30) Ecker, A.; Baum, E.; Friesen, M. A.; Junker, M. A.; Üffing, C.; Schnöckel, H. *Z. Anorg. Allg. Chem.* **1998**, *624*, 513–516.
(31) Klemp, C.; Üffing, C.; Baum, E.; Schnöckel, H. *Z. Anorg. Allg. Chem.* **2000**, *626*, 1787–1791.
(32) Mocker, M.; Robl, C.; Schnöckel, H. *Angew. Chem., Int. Ed. Engl.* **1994**, *33*, 862–863.
(33) Sitzmann, H.; Lappert, M. F.; Dohmeier, C.; Üffing, C.; Schnöckel, H. *J. Organomet. Chem.* **1998**, *561*, 203–208.
(34) Schneider, U.; Ahlrichs, R.; Horn, H.; Schäfer, A. *Angew. Chem., Int. Ed. Engl.* **1992**, *31*, 353–355.
(35) Purath, A.; Dohmeier, C.; Ecker, A.; Schnöckel, H. *Organometallics* **1998**, *17*, 1894–1896.
(36) Schnitter, C.; Roesky, H. W.; Röpken, C.; Herbst-Irmer, R.; Schmidt, H.-G.; Noltemeyer, M. *Angew. Chem., Int. Ed.* **1998**, *37*, 1952–1955.
(37) Purath, A.; Schnöckel, H. *J. Organomet. Chem.* **1999**, *579*, 373–375.
(38) Scheifer, M.; Reddy, N. D.; Roesky, H. W.; Vidovic, D. *Organometallics* **2003**, *22*, 3637–3638.
(39) Li, X.; Brubisic, A.; Stokes, S. T.; Cordes, J.; Ganteför, G. F.; Bowen, K. H.; Kiran, B.; Willis, M.; Jena, P.; Burgert, R.; Schnöckel, H. *Science* **2007**, *315*, 356–358.
(40) Henke, P.; Huber, M.; Steiner, J.; Bowen, K.; Eichhorn, B.; Schnöckel, H. *J. Am. Chem. Soc.* **2009**, *131*, 5698–5704.
(41) Uhl, W. *Naturwissenschaften* **2004**, *91*, 305–319.

(42) Huber, M.; Henke, P.; Schnöckel, H. *Chem.—Eur. J.* **2009**, *15*, 12180–12183.
(43) Vollet, J.; Hartig, J. R.; Schnöckel, H. *Angew. Chem., Int. Ed.* **2004**, *43*, 3186–3189.
(44) Hiller, W.; Klinkhammer, K.-W.; Uhl, W.; Wagner, J. *Angew. Chem., Int. Ed. Engl.* **1991**, *30*, 179–180.
(45) Dohmeier, C.; Mocker, M.; Schnöckel, H.; Lötz, A.; Schneider, U.; Ahlrichs, R. *Angew. Chem., Int. Ed. Engl.* **1993**, *32*, 1428.
(46) Ecker, A.; Weckert, E.; Schnöckel, H. *Nature* **1997**, *387*, 379–381.
(47) Üffing, C.; Baum, E.; Köppe, R.; Schnöckel, H. *Angew. Chem., Int. Ed.* **1998**, *37*, 2397–2400.
(48) Purath, A.; Köppe, R.; Schnöckel, H. *Angew. Chem., Int. Ed.* **1999**, *38*, 2926–2928.
(49) Uhl, W.; Breher, F. *Angew. Chem., Int. Ed.* **1999**, *38*, 1477–1479.
(50) Uhl, W.; Breher, B.; Mbonimana, A.; Gauss, J.; Haase, D.; Lützen, A.; Saak, W. *Eur. J. Inorg. Chem.* **2001**, *2001*, 3059–3066.
(51) Vollet, J.; Burgert, R.; Schnöckel, H. *Angew. Chem., Int. Ed.* **2005**, *44*, 6956–6960.
(52) Ahlrichs, R.; Ehrig, M.; Horn, H. *Chem. Phys. Lett.* **1991**, *183*, 227–233.
(53) Gauss, J.; Schneider, U.; Ahlrichs, R.; Dohmeier, C.; Schnöckel, H. *J. Am. Chem. Soc.* **1993**, *115*, 2402–2408.
(54) Pankewitz, T.; Klopper, W.; Henke, P.; Schnöckel, H. *Eur. J. Inorg. Chem.* **2008**, 4879–4890.
(55) Lammertsma, K.; Leszczyński, J. *J. Phys. Chem.* **1990**, *94*, 2806–2809.
(56) Andrews, L.; Wang, X. *Science* **2003**, *299*, 2049–2052.
(57) Wang, X.; Andrews, L.; Tam, S.; DeRose, M. E.; Fajardo, M. E. *J. Am. Chem. Soc.* **2003**, *125*, 9218–9228.
(58) Baird, N. C. *Can. J. Chem.* **1985**, *63*, 71–76.
(59) Liang, C.; Davy, R. D.; Schaefer, H. F. *Chem. Phys. Lett.* **1989**, *159*, 393–398.
(60) Duke, B. J.; Liang, C.; Schaefer, H. F. *J. Am. Chem. Soc.* **1991**, *113*, 2884–2890.
(61) Szabó, A.; Kovács, A.; Frenking, G. *Z. Anorg. Allg. Chem.* **2005**, *631*, 1803–1809.
(62) Dill, J. D.; von Ragué Schleyer, P.; Pople, J. A. *J. Am. Chem. Soc.* **1975**, *97*, 3402–3409.
(63) ČíŽek, J. *J. Chem. Phys.* **1966**, *45*, 4256–4266.
(64) Crawford, T. D.; Schaefer, H. F. *Rev. Comp. Chem.* **2000**, *14*, 33–136.
(65) Purvis, G. D.; Bartlett, R. J. *J. Chem. Phys.* **1982**, *76*, 1910–1918.
(66) Raghavachari, K.; Trucks, G. W.; Pople, J. A.; Head-Gordon, M. *Chem. Phys. Lett.* **1989**, *157*, 479–483.
(67) Dunning, T. H., Jr. *J. Chem. Phys.* **1989**, *90*, 1007–1023.
(68) Woon, D. E.; Dunning, T. H., Jr. *J. Chem. Phys.* **1993**, *98*, 1358–1371.
(69) Császar, A. G.; Allen, W. D.; Schaefer, H. F. *J. Chem. Phys.* **1998**, *108*, 9751–9764.
(70) East, A. L. L.; Allen, W. D. *J. Chem. Phys.* **1993**, *99*, 4638–4650.
(71) Gonzales, J. M.; Pak, C.; Cox, R. S.; Allen, W. D.; Schaefer, H. F.; Csász, A. G.; Tarczay, G. *Chem.—Eur. J.* **2003**, *9*, 2173–2192.
(72) King, R. A.; Allen, W. D.; Schaefer, H. F. *J. Chem. Phys.* **2000**, *112*, 5585–5592.
(73) Karton, A.; Martin, J. M. L. *Theor. Chem. Acc.* **2006**, *115*, 330–333.
(74) Klopper, W.; Kutzelnigg, W. *J. Mol. Struct.* **1986**, *135*, 339–356.
(75) Helgaker, T.; Klopper, W.; Koch, H.; Noga, J. *J. Chem. Phys.* **1997**, *106*, 9639–9646.
(76) Dunning, T. H., Jr. *J. Chem. Phys.* **1989**, *90*, 1007–1023.
(77) Woon, D. E.; Dunning, T. H., Jr. *J. Chem. Phys.* **1993**, *98*, 1358–1371.
(78) DeYonker, N. J.; Peterson, K. A.; Wilson, A. K. *J. Phys. Chem. A* **2007**, *111*, 11383–11393.
(79) Weinhold, F. In *Encyclopedia of Computational Chemistry*; von Ragué Schleyer, P., Allinger, N. L., Clark, T., Gasteiger, J., Kollman, P. A., Schaefer, H. F., Schreiner, P. R., Eds.; John Wiley and Sons, Ltd.: New York, 1998; Vol. 3, pp 1792−1811.
(80) Godbout, N.; Salahub, D. R.; Andzelm, J.; Wimmer, E. *Can. J. Chem.* **1992**, *70*, 560.
(81) Runge, E.; Gross, E. K. U. *Phys. Rev. Lett.* **1984**, *52*, 997–1000.
(82) Becke, A. D. *J. Chem. Phys.* **1993**, *98*, 5648–5652.
(83) Lee, C.; Yang, W.; Parr, R. G. *Phys. Rev. B* **1988**, *37*, 785–789.
(84) Dunning, T. H., Jr.; Hay, P. J. In *Methods of Electronic Structure Theory*; Schaefer, H. F., Ed.; Plenum Press: New York, 1977; Vol. 2, pp 1−27.
(85) Bergner, A.; Dolg, M.; Küchle, W.; Stoll, H.; Preuss, H. *Mol. Phys.* **1993**, *80*, 1431–1441.
(86) Shao, Y.; et al. *Phys. Chem. Chem. Phys.* **2006**, *8*, 3172–3191.
(87) Werner, H. J. et al. *MOLPRO*, version 2006.1, 2006.
(88) Reed, A. E.; Weinhold, F.; Curtiss, L. A.; Pochatko, D. J. *J. Chem. Phys.* **1986**, *84*, 5687–5705.
(89) Reed, A. E.; Weinhold, F. *J. Chem. Phys.* **1983**, *78*, 4066–4073.
(90) Foster, J. P.; Weinhold, F. *J. Am. Chem. Soc.* **1980**, *102*, 7211–7218.
(91) Reed, A. E.; Weinstock, R. B.; Weinhold, F. *J. Chem. Phys.* **1985**, *83*, 735–746.
(92) Weinhold, F.; Landis, C. *Valency and Bonding A Natural Bond Orbital Donor-Acceptor Perspective*, 1st ed.; Cambridge University Press: Cambridge, UK, 2005.
(93) Mulliken, R. S. *J. Phys. Chem.* **1952**, *56*, 801–822.
(94) Mulliken, R. S. *J. Am. Chem. Soc.* **1952**, *74*, 811–824.
(95) Urban, J.; Schreiner, P. R.; Vacek, G.; von Ragué Schleyer, P.; Huang, J. Q.; Leszczyński, J. *Chem. Phys. Lett.* **1997**, *264*, 441–448.